Advances in Geo-Energy Research

Vol. 6, No. 3, p. 181-191, 2022

Original article

Leakage simulation and acoustic characteristics based on acoustic logging by ultrasonic detection

Jingcui Li[1,2], Jifang Wan[2]*, Tingting Wang[3], Guangjie Yuan[2], Maria Jose Jurado[4], Qing He[3]

[1]*College of Resources and Safety Engineering, Chongqing University, Chongqing 400044, P. R. China*

[2]*CNPC Engineering Technology R&D Company Limited, Beijing 102206, P. R. China*

[3]*School of Energy Power and Mechanical Engineering, North China Electric Power University, Beijing 102206, P. R. China*

[4]*Geosciences Barcelona CSIC, Spanish National Research Council, Barcelona 08028, Spain*

Keywords:
Acoustic logging
well logging
leakage
ultrasound
simulation
numerical modelling

Cited as:
Li, J., Wan, J., Wang, T., Yuan, G., Jurado, M. J., He, Q. Leakage simulation and acoustic characteristics based on acoustic logging by ultrasonic detection. Advances in Geo-Energy Research, 2022, 6(3): 181-191.
https://doi.org/10.46690/ager.2022.03.02

Abstract:
The detection of casing leakage in oil and gas wells or water injection wells is an important element of wellbore integrity management. Ultrasonic technology is suitable to detect and identify the position of leakage in oil and gas well shafts, providing engineering guidance for subsequent treatment. In this paper, the finite element calculation model of casing leakage in oil and gas wells is established by using the computational fluid dynamics method, and the large eddy simulation model and Ffowcs Williams-Hawkings acoustic model are utilized to simulate the casing leakage condition. The acoustic pressure signals of each monitoring point on the inner axis of the pipeline are obtained, and the influences of the pipeline pressure difference, the leakage hole diameter and the pipeline fluid on the leakage acoustic field are analyzed. The simulation results indicate that the acoustic pressure level measured on the pipeline axis rises with the increase of pipeline pressure difference and leakage hole diameter. The size and variation rule of acoustic pressure level also vary with the type of pipeline fluid. Overall, the results obtained show that ultrasonic logging can accurately locate and detect tubing leakage, and they provide theoretical guidance for practical casing leakage detection, assisting with wellbore integrity management.

1. Introduction

Casing oil and gas leakage has become a global concern because of its adverse impact on the ecosystem (Shahmirzaee et al., 2019). It often occurs in practical engineering applications, not only causing energy loss and environmental pollution, but also threatening the safety of residents (Mahmutoglu and Turk, 2019; Zhang and Weng, 2020; Rai et al., 2021). Therefore, casing leakage detection is a crucial part of well integrity management (Datta et al., 2016; Ning et al., 2021; Zhang et al., 2021c). To avoid accidents due to oil and gas pipeline leakage, the exact location and quantity of leakage must be identified (Lalitha et al., 2020; Jahanian et al., 2021). Most leakages are small at the initial stage and will increase over time. Locating leakages in the early stages of leakage development can reduce remediation costs. Meanwhile, very small wellbore leaks (<3.785 L/min) are difficult to detect through conventional leakage detection techniques, such as multi-arm caliper logging, acoustic televiewer and other borehole imaging techniques, electromagnetic flaw detection logging, rotor flowmeter, gradient well temperature logging, downhole cameras, thermal neutron attenuation logging, or noise logging (Piltan and Kim, 2019; Moosavi et al., 2020; Zhang et al., 2021a). When the leakage is small, the temperature, pressure, flow velocity and other characteristics around the wellbore leakage point change little, which is often beyond the resolution threshold of the fluid temperature, flow, and pressure logging tools. Conventional noise logging can only detect the acoustic energy in fixed-point measurement mode in the acoustic band generated by the liquid or gas at the leakage point.

Yandy Scientific Press

*Corresponding author.
E-mail address: lijingcuidri@cnpc.com.cn (J. Li); wanjifang@126.com (J. Wan); yuyu@ncepu.edu.cn (T. Wang); ygjdri@cnpc.com.cn (G. Yuan); mjjurado@csic.es (M. J. Jurado); heq@ncepu.edu.cn (Q. He).

Received February 21, 2022; revised March 15, 2022; accepted March 16, 2022; available online March 19, 2022.

In addition, because of the influence of other distant noise sources, there is a multi-solution of logging interpretation. Downhole cameras (such as video system logging tools) are effective in detecting leakages and diagnosing other problems, but they require the high resolution of fluids or gases in the well (Cao et al., 2021; Shi et al., 2022). In addition, leakages that occur outside the multilayer string cannot be located using conventional borehole leak detection techniques. Therefore, under the modern requirements of safety and environmental protection, new logging methods with wider application scope and more accurate measurement results are urgently needed (Lu et al., 2020).

Gas leakage in the wellbore/pipeline will produce vibrations in three frequency bands: infrasonic, sonic and ultrasonic (Zhang et al., 2020). Compared with the acoustic wave energy of infrasound and sonic frequencies, ultrasound has good directivity, strong penetrating ability and the ease of recording more concentrated acoustic energy (Hudson et al., 2021). Moreover, ultrasound has the advantage of relatively short propagation distance, and when an ultrasonic signal is detected in a given ultrasonic frequency band, this indicates that the leakage location is closer to the source. These characteristics make ultrasound ideal for accurate leakage detection. Accordingly, ultrasound technology has been developed for many years for leakage detection in production equipment such as valves and wellhead devices.

Domestic and abroad scholars have carried out exploration and research on ultrasonic detection of pipeline/tubing leakage. Mei et al. (2021) conducted pipeline leakage detection experiments to study pipeline leakage problems under different pore sizes and pipeline pressures, and they verified the feasibility of the leakage detection method based on acoustic emission technology combined with a frequency-domain feature extraction algorithm. Xu et al. (2021) performed leakage experiments on two-phase flow pipelines and proved that acoustic emission technology and BP neural network identification have high accuracy in leakage detection in two-phase flow pipelines. Quy and Kim (2020) proposed a reliable method to detect leaks and recognize their various sizes in a gas pipeline based on the spectral portrait of acoustic emission signals. Zhang et al. (2021b) introduced the overall design of a new acoustic logging tool while drilling, tested the tool, and obtained qualified data. Shan et al. (2021) coupled the hybrid neural network prediction logging curve, carried out practice and evaluation in the field, and achieved high prediction accuracy. Keramat and Duan (2021) developed a new technique for leak detection, called Matched-Field Processing. Fedotov et al. (2021) studied the detection band of laser fluorescence sensor to detect oil pipeline leakage. Fu et al. (2020) established the relationship between pressure distribution and leakage parameters through simulation and verified it through experiments. Adegboye et al. (2021) systematically analyzed the effects of leak size, longitudinal leak location, multiple leaks, and axial leak locations on the pressure gradient, flow rate and volume fraction in the pipeline. Ghosh and Saha (2021) simulated a slit similar to a pipe crack and compared it with the experimental results to prove the validity of the analysis. Yuan et al. (2020) studied the generation and propagation of negative waves in pipeline leakage through computational fluid dynamics simulation and proposed a dimensionless correlation equation between pipeline pressure and leakage aperture. Doshmanziar et al. (2020) proposed a leakage detection method for long-distance pipelines based on nonlinear modeling and verified its effectiveness. Zeng and Luo (2019) conducted a numerical simulation of pipeline leakage conditions and studied the influence of pipeline diameter, inlet mass flow rate, main length, Zadkarami et al. (2017) utilized a multi-layer perceptron neural network and the Dempster-Shafer technique to determine the size and location of leakage, and other factors on the flow phenomenon near the location of leakage.

It is expected that ultrasound logging is effective in detecting the leakage and channeling of downhole string or annulus in oil and gas wells. Therefore, based on the successful application experience of ultrasonic surface leakage detectors and the excellent characteristics of ultrasonic transmission, this paper theoretically explores the development of downhole ultrasonic detectors. First, the design modeler (DM) module in ANSYS software is used to establish a three dimension (3D) model of the casing, and the large eddy simulation model in Fluent module is employed to simulate the flow field changes of casing leakage under different conditions. Then, the acoustic field variation of casing leakage under different conditions is simulated by the Ffowcs Williams-Hawkings (FW-H) model. Finally, the influence of pipeline pressure difference, leakage hole diameter, and pipeline fluid on leakage acoustic field is compared and analyzed by the acoustic pressure level spectrum diagram measured at the monitoring point on the pipe axis, and the conclusions are drawn.

2. Fluid acoustic theory

All leakage release a certain amount of ultrasonic energy, which is related to the size of the leak channel and differential pressure, and different leakage produce different energy spectra and different amplitudes. The human ear can hear acoustic waves at frequencies between 20 and 20,000 Hz. Ultrasonic frequency is greater than 20,000 Hz, which is a high-frequency short-wave signal. It is directional and cannot be heard directly by the human ear. Therefore, ultrasonic leakage detection can be used in noisy environments, and the air tightness detection of casings and tubings can be realized by using ultrasonic waves. When an oil casing leaks, the flow in the pipeline jets out of the leakage hole, forms turbulence near the leakage hole, and interacts with the pipe wall, resulting in noise due to the intense velocity and pressure pulsation.

Aeroacoustics is the basic theory for studying the acoustic waves generated by pipeline leakage (Zhang et al., 2017; Karthik et al., 2021), which mainly examines the principle of acoustics produced by the fluid-solid or fluid-fluid interaction. The basic equations of the theory are derived from continuity equations and momentum equations.

The continuity equation, as the mathematical expression of the law of mass conservation, is satisfied by the fluid flow and is expressed as

$$\frac{\partial \rho}{\partial t}+\frac{\partial(\rho u)}{\partial x}+\frac{\partial(\rho v)}{\partial y}+\frac{\partial(\rho w)}{\partial z}=0 \tag{1}$$

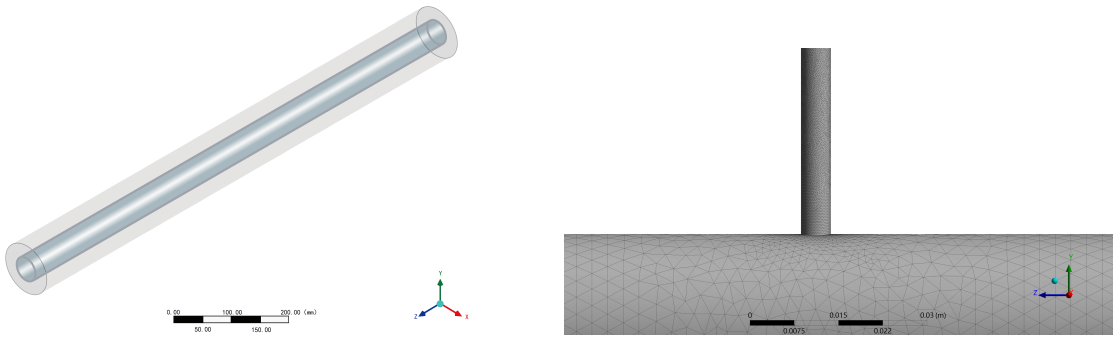

(a) Casing model

(b) Local amplification near the leak hole

Fig. 1. Schematic of casing model.

where ρ represents the fluid density, kg/m^3; u, v and w represent the velocity components of the fluid on the x, y, and z, respectively, m/s.

The momentum equation is the mathematical expression of momentum conservation law, also known as Navier and Stokes equations, expressed in the rectangular coordinate system as

$$\begin{cases} \dfrac{\partial(\rho u)}{\partial t}+\dfrac{\partial(\rho uu)}{\partial x}+\dfrac{\partial(\rho uv)}{\partial y}+\dfrac{\partial(\rho uw)}{\partial z} \\ \quad =-\dfrac{\partial p}{\partial x}+\mu\left(\dfrac{\partial^2 u}{\partial x^2}+\dfrac{\partial^2 u}{\partial y^2}+\dfrac{\partial^2 u}{\partial z^2}\right)+F_x \\ \dfrac{\partial(\rho v)}{\partial t}+\dfrac{\partial(\rho uv)}{\partial x}+\dfrac{\partial(\rho vv)}{\partial y}+\dfrac{\partial(\rho vw)}{\partial z} \\ \quad =-\dfrac{\partial p}{\partial y}+\mu\left(\dfrac{\partial^2 v}{\partial x^2}+\dfrac{\partial^2 v}{\partial y^2}+\dfrac{\partial^2 v}{\partial z^2}\right)+F_y \\ \dfrac{\partial(\rho w)}{\partial t}+\dfrac{\partial(\rho uw)}{\partial x}+\dfrac{\partial(\rho vw)}{\partial y}+\dfrac{\partial(\rho ww)}{\partial z} \\ \quad =-\dfrac{\partial p}{\partial z}+\mu\left(\dfrac{\partial^2 w}{\partial x^2}+\dfrac{\partial^2 w}{\partial y^2}+\dfrac{\partial^2 w}{\partial z^2}\right)+F_z \end{cases} \tag{2}$$

where μ represents dynamic viscosity, N·s/m^2; F_x, F_y, F_z are the component forces of the resultant force in the direction of x, y and z, respectively, N.

Based on the above equation, in 1952, Lighthill proposed the equation of airflow motion sound as follows

$$\begin{cases} \dfrac{\partial^2 p'}{\partial t^2}-c^2\nabla^2 p'=\dfrac{\partial^2 T_{ij}}{\partial x_i \partial x_j} \\ T_{ij}=\rho u_i u_j+p'\delta_{ij}-c^2 p'\delta_{ij}-\tau_{ij} \end{cases} \tag{3}$$

where $p'=p-p_0$ represents far-field sound pressure, Pa; c represents far-field sound speed, m/s; T_{ij} represents Lighthill stress tensor; u_i and u_j are the velocity components of the flow field in the x and y directions, respectively, m/s; δ_{ij} denotes Kronecker number; τ_{ij} is the viscous stress tensor of fluid.

However, the Lighthill equation is derived from the assumption of free space without considering the effect of solid boundary. On this basis, Curle proposed the Lighthill-Curle equation in 1955, which made it possible to study the phenomenon of object acoustics in turbulent flow. Later, Ffowcs and Hawkings further extended the Lighthill-Curle equation to study the acoustic phenomenon of the interaction between solid boundary and fluid, and proposed a relatively common result–the FW-H equation, expressed as follows (Sarallah and Mohammad, 2021)

$$\begin{aligned} \frac{1}{c}\frac{\partial^2 p'}{\partial t^2}-\nabla^2 p' &= \frac{\partial}{\partial t}\left\{\left[\rho_0 v_n+\rho\left(u_n-v_n\right)\right]\delta(f)\right\} \\ &\quad -\frac{\partial}{\partial x_i}\left\{\left[\rho u_i\left(u_n-v_n\right)+p'\delta_{ij}-\sigma_{ij}\right]\delta(f)\right\} \\ &\quad +\frac{\partial^2}{\partial x_i \partial x_j}\left[T_{ij}H(f)\right] \end{aligned} \tag{4}$$

where u_n and v_n represent the fluid velocity component perpendicular to the integrating surface and the moving velocity component of the integrating surface, respectively, m/s; $\delta(f)$ is Dirac function; u_i represents the velocity component of the fluid in the x_i direction, m/s; σ_{ij} is the shear stress tensor of fluid; and $H(f)$ denotes Heaviside function.

In Eq. (4), the three items on the right side of the medium sign are acoustic source terms. The first item is a monopole acoustic source, which is the acoustic source generated when the mass or heat is uneven in the medium. The second item is the dipole acoustic source, which is the acoustic source formed by the reaction force generated by the higher-velocity fluid and the obstacles in the fluid. The third is the quadrupole acoustic source, which is the stress source formed by the viscous stress of turbulent fluid.

3. Acoustic numerical simulation of casing leakage

3.1 Mathematical model

In this paper, the DM module in ANSYS is used to establish a 3D casing model, as shown in Fig. 1(a). The casing model is mainly composed of four parts: pipe, pipe wall and annulus, and a leakage hole located on the outer wall of the casing. The casing has a total diameter of 110 mm and inner diameter of 57 mm, the thickness of the pipe wall is 2.5 mm, and the total length of the casing model is 1 m. The leakage hole is located at the middle point of the outer wall of the casing, and has a diameter of 0.2 mm and height of 2.5 mm, which is equal to the thickness of the pipe wall.

After constructing the 3D model, it was imported into ANSYS Meshing for grid division. Tetrahedral grid was used for the whole model grid, as shown in Fig. 1(b). Grid en-

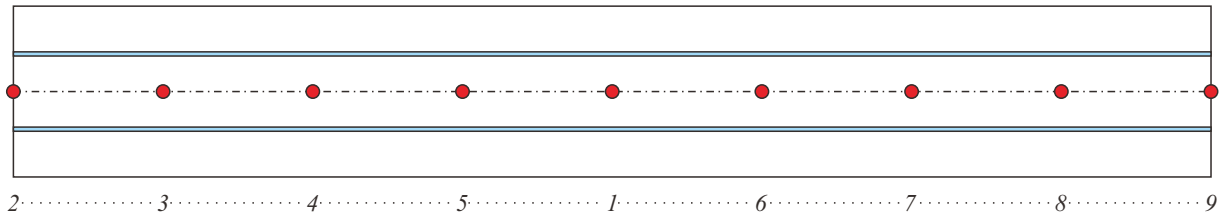

Fig. 2. Position of pipeline axis at each monitoring point.

cryption was carried out near the location of the leak hole, and after grid independence verification, the number of grids was determined to be about 1 million, which could meet the accuracy requirements.

3.2 Calculation settings

The flow field simulation calculation adopts the large eddy simulation model, which simulates two working fluids: air and methane. For simplicity, both working media are assumed to be incompressible ideal gases. To study the influence of pipeline pressure difference and leakage hole diameter on the flow field and acoustic field, the leakage hole diameters considered are 0.085 mm, 0.15 mm, 0.2 mm and 0.235 mm, and the pipeline pressure difference values tested are 2 MPa, 3 MPa, 4 MPa, and 5 MPa. In the model, the outlet of the leakage hole is an atmospheric pressure environment. The pressure inlet is used for annulus and pipe inlet, the pressure outlet is used for the outlet, and the pipe wall is solid without a slip boundary. It is assumed that the fluid flow process in the whole pipeline is incompressible adiabatic flow, and the temperature in the pipeline and annulus is constant at 25 °C.

In this paper, the aerodynamic acoustics theory, i.e., FW-H equation is employed to simulate the acoustic field. The acoustic source and acoustic propagation are calculated based on the flow field result data. The surface of the leakage hole is set as the acoustic source area, and the interior of the pipe and annulus are set as the acoustic propagation area. The frequency range of acoustic field simulation is set as 0∼100 kHz by setting the time step as 5×10^{-6} s. The monitoring points are uniformly set on the pipe axis to measure the acoustic pressure parameters at each position. Taking the central point of one end of the pipeline as the origin of coordinates, the monitoring points are located on the z-axis with mm as the unit. The coordinates of individual monitoring points are 1(0, 0, 500), 2(0, 0, 1000), 3(0, 0, 875), 4(0, 0, 750), 5(0, 0, 625), 6(0, 0, 375), 7(0, 0, 250), 8(0, 0, 125), and 9(0, 0, 0), as shown in Fig. 2.

4. Results and discussion

The most common method to detect casing leakage is a series of casing inspections based on ultrasonic logging. However, through conventional leak detection technology, it is difficult to detect very small wellbore leaks (less than 3.785 L/min), and it is not possible to locate leaks outside the multilayer pipe string. The simulation calculation is based on small leakage, with the leakage aperture set to 0.085 mm, 0.15 mm, 0.2 mm or 0.235 mm. The leakage also occurs on the annular casing outside the pipeline. The flow field change during annular leakage and the acoustic pressure generated by the leakage measured inside the pipeline are calculated, so as to provide a theoretical basis for the detection and location of small leaks. The experimental validation is also based on the relatively obvious acoustic pressure spectrum measured by small leakage and casing detection. Using both theoretical analysis and experimental measurement, the leakage detection task is better simulated.

4.1 Flow field

For the simulation conditions, the external pressure of the pipeline is set as 1 atm, that is, the outlet pressure p_2 of the leakage hole is 1 atm, and the pressure inside the pipeline is 2-5 MPa, so the pressure ratio between the interior and exterior of the pipeline is

$$v = \frac{p_2}{p_1} = 0.020 \sim 0.051 \tag{5}$$

The adiabatic index $k = 1.4$ of the pipeline fluid medium is substituted into Eq. (1) to get $v_{cr} = 0.528$, and obviously, $v < v_{cr}$. Therefore, for the various simulation conditions, the flow of fluid at the leakage hole is in a critical state, that is, the flow velocity at the outlet of the leakage hole is the local acoustic speed under the corresponding pressure. Fig. 3 shows the flow field velocity cloud diagram at the outlet of the leakage hole under the condition of 0.15 mm diameter and 3 MPa pressure difference between the interior and exterior of the pipe. The flow velocity at the outlet of the leakage hole is 366 m/s.

The main factors influencing the flow rate at the leakage hole outlet are the pressure difference between the interior and exterior of the pipe and the diameter of the leakage hole. Since this study is principally aimed at the simulation of small leakage in the pipeline, the leakage hole apertures of 0.085 mm, 0.15 mm, 0.2 mm or 0.235 mm are selected for calculation, and the pressure difference condition of the pipeline is 2 MPa, 3 MPa, 4 MPa or 5 MPa, respectively. Under the condition of the same leak hole diameter, the flow velocity at the leak hole outlet obtained by simulation is sorted out and the error value is calculated, as shown in Table 1.

Given the calculation conditions of this paper, the influence of pressure difference change on the outlet flow rate of leakage hole is not obvious. Under the same aperture but different pressure differences, the leakage hole outlet velocities calculated by software are roughly the same. It can be seen from Table 1 that the maximum relative error of the outlet flow

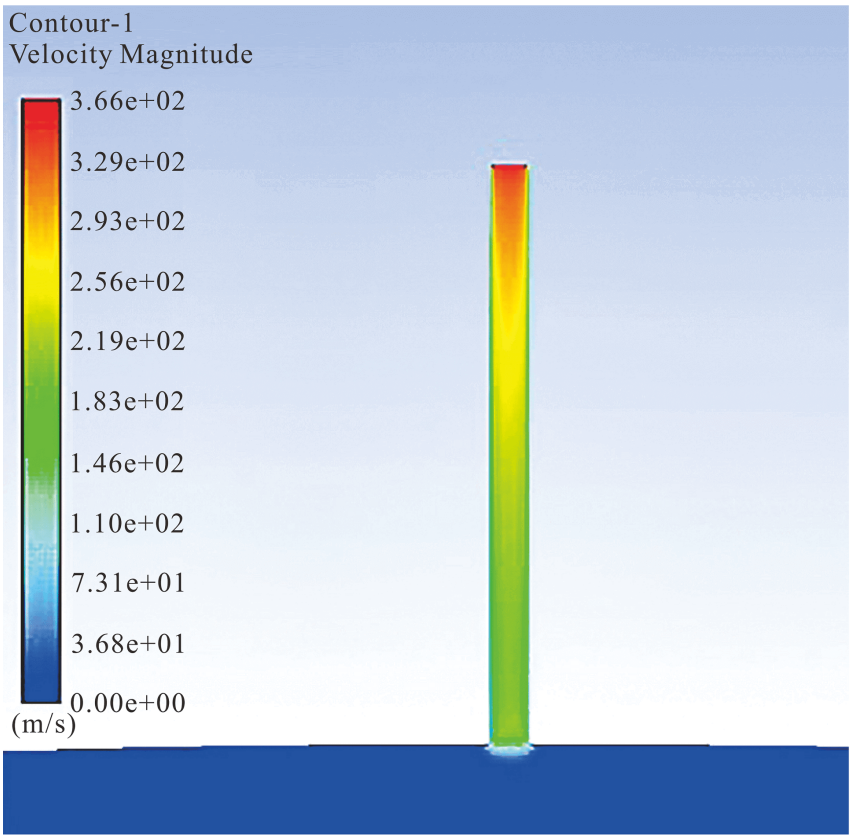

Fig. 3. Outlet velocity cloud diagram of 0.15 mm diameter leakage hole under 3 MPa pressure difference.

Table 1. Outlet flow velocity of leak hole under different pore diameters and pressure differences.

Leakage aperture, mm	Pressure difference, MPa	Leakage outlet flow rate, m/s	Error, %
0.085	2	375	1.05
	3	379	0.00
	4	369	2.60
	5	369	2.60
0.150	2	366	0.00
	3	366	0.00
	4	365	0.27
	5	364	0.54
0.235	2	359	0.00
	3	359	0.00
	4	359	0.00
	5	358	0.28

velocity of leakage hole under different aperture conditions is 2.6% (aperture: 0.085 mm), 0.54% (aperture: 0.15 mm) and 0.28% (aperture: 0.235 mm), respectively, using 3 MPa outlet flow velocity as the reference value. Thus, it can be considered that the flow rate at the outlet of the leakage hole is fairly consistent.

In contrast, under the calculation conditions, the influence of leakage hole diameter on outlet velocity is more obvious. As can be seen from Table 1, the flow rate at the outlet of the leakage hole decreases with the gradual increase in the leakage hole diameter. The outlet velocity of the leakage hole is close to the local acoustic speed under the corresponding pressure, and it decreases with the increase of leakage hole aperture.

Table 2. Average SPL of monitoring points under the condition of 0.2 mm aperture and 3 MPa pipe interior-exterior pressure difference.

Point	2	3	4	5	1	6	7	8	9
Average SPL/dB	-8.14	-5.46	-1.52	2.61	-25.29	2.30	-1.07	-5.01	-7.76

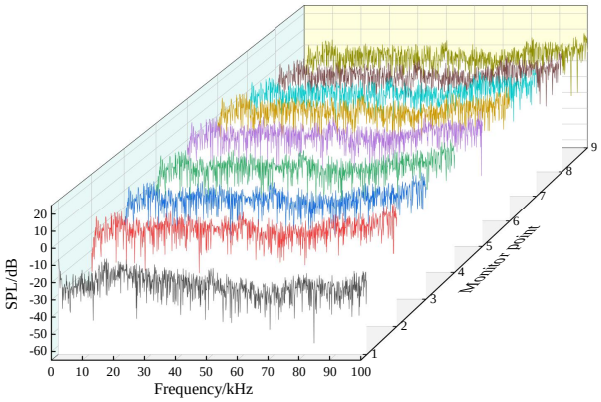

Fig. 4. 3D acoustic pressure spectrum diagram.

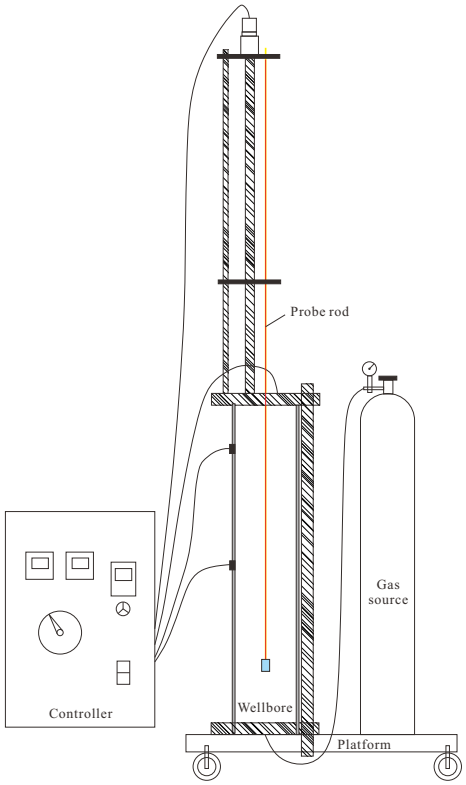

Fig. 5. Wellbore leakage simulator.

4.2 Acoustic field

Fig. 4 presents the 3D acoustic pressure spectrum diagram at each monitoring point under the condition of 0.2 mm aperture and 3 MPa pipe internal and external pressure difference. The monitored parameter is sound pressure level (SPL), and the reference acoustic pressure is 2×10^{-5} Pa. In this calculation, we set a total of 9 acoustic pressure monitoring points evenly distributed on the axis, with the distance of 125 mm between two adjacent monitoring points. Monitoring point 1 is located on the position axis directly below the leakage hole, and the other monitoring points are distributed symmetrically.

The average acoustic pressure level is obtained by averaging each acoustic pressure level data within the calculation frequency, so as to visualize the acoustic pressure level change of each monitoring point. The average acoustic pressure level of all monitoring points from Fig. 4 is shown in Table 2, where the order of the monitoring point numbers is the same as that in Fig. 2.

Fig. 4 and Table 2 show the distribution of acoustic pressure values measured at each monitoring point. The acoustic pressure measured at monitoring point 1 is generally lower than that measured at other monitoring points. The acoustic pressure charts measured at two symmetrical monitoring points, such as 5, 6 (or 4, 7, or 3, 8, or 2, 9), have a relatively high coincidence degree. Moreover, the acoustic pressure values measured at the monitoring points show a trend of gradual decline according to 5→4→3→2 and 6→7→8→9, which is consistent with the transmission trend of acoustic waves. It can be concluded that the distribution of acoustic pressure values is as follows: the acoustic pressure value directly below the leakage hole can be characterized by a typical or characteristic pressure drop. The value of acoustic pressure transmitted from the leakage hole to both ends of the pipeline shows a trend of gradual decline and presents a roughly symmetrical distribution, which is in line with the theory of acoustic propagation.

4.3 Experiment

In order to verify the results of the above simulation calculation and analysis, a wellbore leakage simulation test device was built to simulate various leakage conditions of a natural gas wellbore under real formation conditions. The schematic diagram of the structure and principle of the wellbore leakage simulation device is shown in Fig. 5.

The laser machining method was used to produce the leakage hole to meet the aperture requirements. Multiple groups of tests were carried out on the same leakage hole. The pressure in the wellbore was individually set as 1 MPa, 2 MPa, 3 MPa or 4 MPa, and the outside of the wellbore was atmospheric pressure environment. The gain of the leakage signal processing circuit was fixed at 2,000 times. The detection process included the following steps: under the condition that the leakage pressure difference remains unchanged, the leakage probe rod is moved to each measurement position in turn. The leakage acoustic signal detected by the detection circuit in each position is measured and recorded by a computer, and

the acoustic value is obtained by analysis. Eight tests were carried out at each position, and the acoustic values at this position were obtained by averaging the 8 groups of measured acoustic data to eliminate the influence of random interference on the test results.

Fig. 6 shows the change curve of acoustic pressure measured by ultrasonic signal in the simulation test, with the position of wellbore clearly seen. The ultrasonic acoustic pressure signal is the largest at the leakage hole, and decays rapidly as the ultrasonic sensor moves away from the leakage hole. Thus, it can be seen that the leakage hole can be accurately located on the tubing through ultrasonic detection.

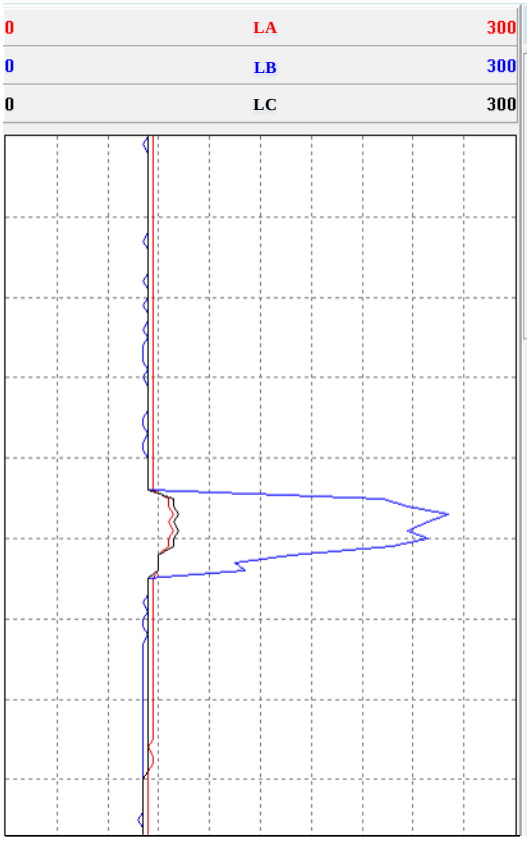

Fig. 6. Ultrasonic acoustic pressure curves of wellbore leakage detection.

In Fig. 6, LA, LB and LC stand for three different filters: LA denotes low frequency band with a center frequency of 20 kHz; LB denotes mid frequency band with a center frequency of 40 kHz; LC denotes high frequency band with a center frequency of 60 kHz. Under the experimental conditions of this paper, the filter with a center frequency of 40 kHz is more sensitive, hence the acoustic pressure amplitude of LB is the largest.

4.4 Pressure difference

In order to study the influence of pipeline internal and external pressure difference on the acoustic field, four different pressure difference conditions of 2 MPa, 3 MPa, 4 MPa and 5 MPa were considered, and monitoring point 1 was set on the pipeline axis directly below the leakage hole to measure the acoustic pressure value. Fig. 7 shows the change of acoustic pressure spectrum at measuring point 1, with the pressure difference between the interior and exterior of the pipeline.

As can be seen from Fig. 7, in models with different leakage hole sizes, although the acoustic pressure values are different, the variation trend of the acoustic pressure values with the pressure difference between the interior and exterior of pipeline is consistent. As the pressure difference increases, the acoustic pressure value gradually increases, and with the increase of pressure difference, the rate of acoustic pressure increase becomes gradually smaller. The maximum sound pressure value almost appears between 15∼22 kHz. It is concluded that, under the condition of constant leakage hole diameter, the acoustic pressure on the axis below the leakage hole increases gradually with the pressure difference between the interior and exterior of the pipeline, and the results are consistent.

4.5 Leakage aperture

In order to study the influence of leakage hole diameter on the acoustic field, four different leakage hole diameter conditions of 0.085 mm, 0.15 mm, 0.2 mm and 0.235 mm are considered. The monitoring point on the pipe axis is directly below the leakage hole to measure the acoustic pressure value.

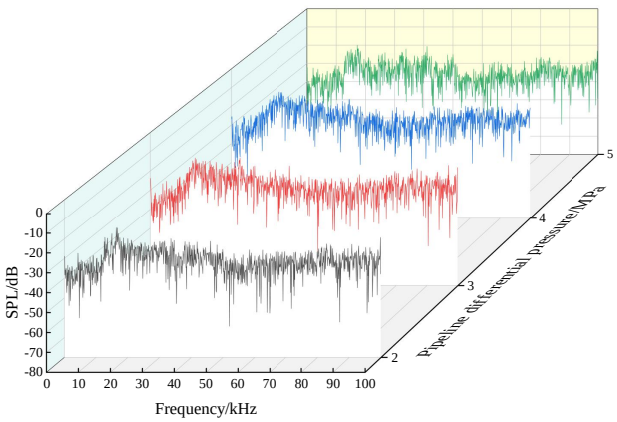

(a) Leakage aperture of 0.085 mm

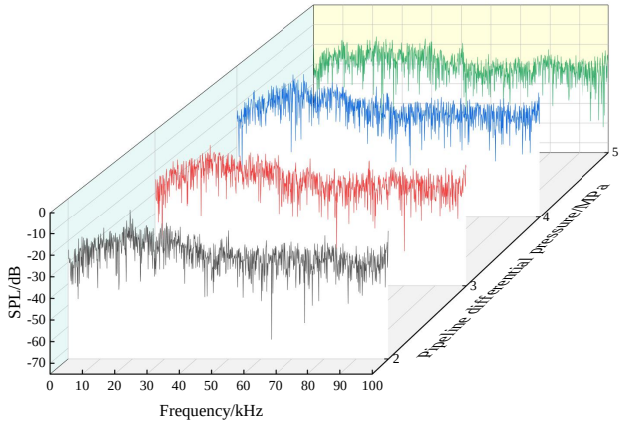

(b) Leakage aperture of 0.15 mm

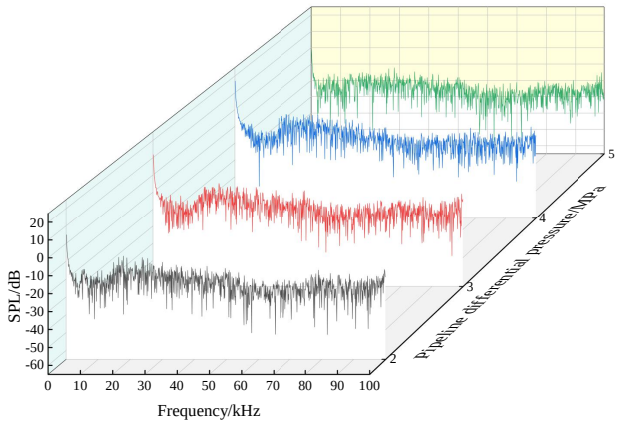

(c) Leakage aperture of 0.235 mm

Fig. 7. Relationship between the acoustic pressure spectrum at measuring point 1 and the pressure difference between the interior and exterior of pipeline.

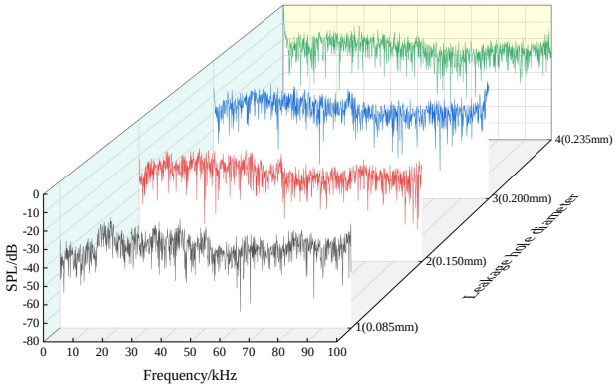

(a) Pressure difference of 2 MPa

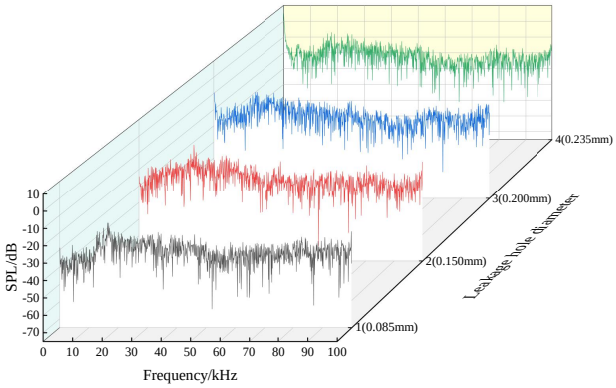

(b) Pressure difference of 3 MPa

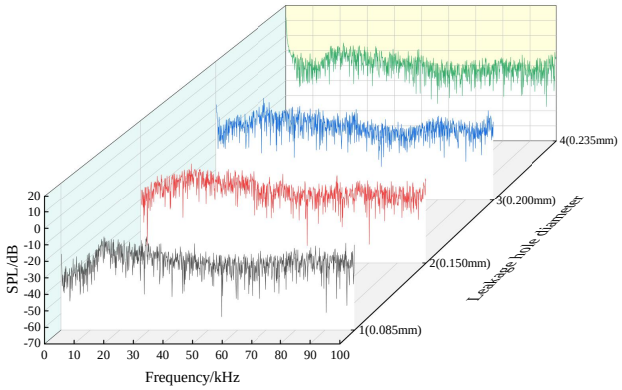

(c) Pressure difference of 4 MPa

Fig. 8. Relationship between acoustic pressure spectrum at measuring point 1 and the leakage hole aperture.

As can be seen from Fig. 8, under different pipeline interior and exterior pressure differences, although the acoustic pressure values are different, the changing trend of acoustic pressure values are consistent with the leakage hole aperture. In both cases, the acoustic pressure increases gradually with the increase of leakage hole aperture, and the maximum acoustic pressure value nearly appears between 14∼21 kHz. It is therefore concluded that, under the condition of constant pipeline interior and exterior pressure difference, the acoustic pressure value on the axis below the leakage hole rises gradually with the increase of leakage hole aperture, and the results are consistent.

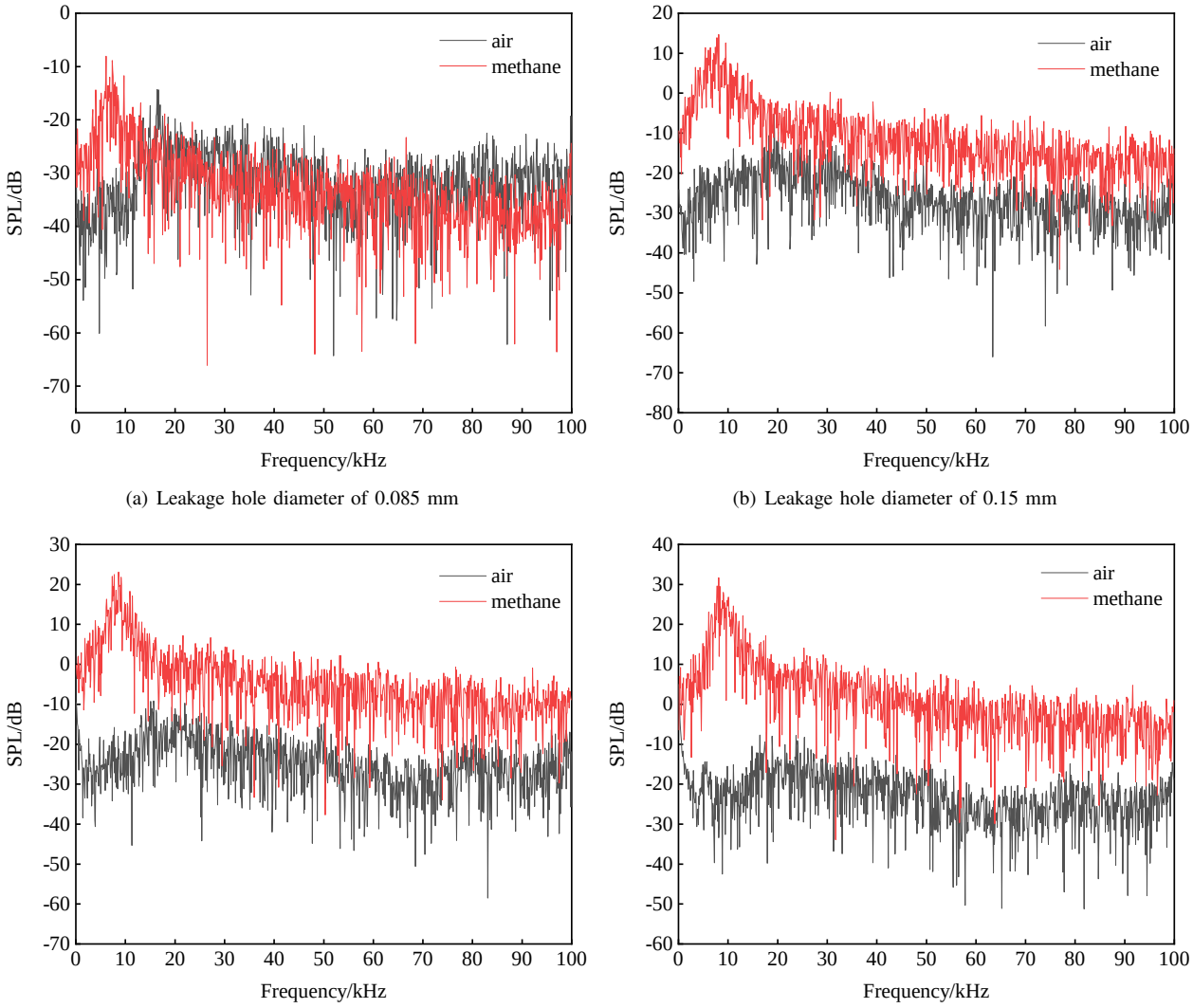

(a) Leakage hole diameter of 0.085 mm

(b) Leakage hole diameter of 0.15 mm

(c) Leakage hole diameter of 0.2 mm

(d) Leakage hole diameter of 0.235 mm

Fig. 9. Acoustic pressure spectrum diagrams of monitoring point 1 under different pore sizes and fluids with a pressure difference of 3 MPa.

4.6 Working conditions

In order to study the influence of fluid type in the casing on the acoustic field, two different fluid conditions of ideal air and methane are considered, and the filling fluid in the annulus is air. Monitoring point 1 is set on the pipe axis directly below the leakage hole to measure the acoustic pressure value. The comparison of the leakage acoustic pressure spectra of the two working conditions at the measuring point is shown in Fig. 9.

As can be seen from Fig. 9, under the condition of constant leakage hole diameter and pressure difference, the measured acoustic pressure values on the axis below the leakage hole have obvious variation between different fluids in the casing. The value of difference is smaller when the leakage hole diameter is small, and it rises with the increase of leakage hole diameter. This suggests that the methane condition is more sensitive to the change of leakage hole diameter than the ideal air condition. Fluid noise is formed due to pressure or velocity pulsation caused by fluid turbulent motion. For methane gas and ideal air, the physical properties of the two are different: considering the flow in the same casing model with the same pressure difference between the interior and exterior of the pipeline, both the turbulent motion situation and the resulting pressure or velocity pulsations differ. It can be seen that, with the change of fluid, the acoustic pressure diagram of leakage condition also changes, and the change of the leakage hole aperture has a more obvious effect for methane gas than for air as a flow medium.

5. Conclusions

1) Under the leakage condition calculated, the changes of flow field at the leakage hole are roughly the same. The outlet velocity of the leakage hole is equal to the local acoustic speed under the corresponding pressure within the allowable error range, and it rises with the increase of the pressure difference between the interior and exterior of the pipe.

2) Under the leakage condition calculated, the variation of the acoustic field at the leakage hole is also consistent. The acoustic pressure directly below the leakage hole drops suddenly, while the acoustic pressure transmitted from the leakage hole to both ends of the pipe gradually drops.
3) According to the comparison of various working conditions calculated, the acoustic pressure value directly below the leakage hole increases with the rise of pressure difference between the interior and exterior of the pipeline, and it increases with the enlargement of leakage hole aperture. Under different flow medium conditions, the measured acoustic pressure values have obvious differences, and they increase with the enlargement of leakage hole diameter. It can be seen that the change of leakage hole aperture has a more obvious effect under methane than air medium.

Acknowledgement

The authors would like to gratefully acknowledge the financial support from the CNPC scientific research and technology development project "Research on key technologies of compressed air and hydrogen energy storage engineering in salt cavern" (No. 2021DJ5402) and "Tubing pipe leak detection tool upgrade and field test" (No. kt2020-16-05).

Conflict of interest

The authors declare no competing interest.

References

Adegboye, M. A., Karnik, A., Fung, W. K. Numerical study of pipeline leak detection for gas-liquid stratified flow. Journal of Natural Gas Science and Engineering, 2021, 94: 104054.

Cao, J., Zhang, J., Yu, X., et al. Detection of pressure relief valve leakage by tuning generated sound characteristics. Process Safety and Environmental Protection, 2021, 148: 664-675.

Datta, S., Sarkar, S. A review on different pipeline fault detection methods. Journal of Loss Prevention in the Process Industries, 2016, 41: 97-106.

Doshmanziari, R., Khaloozadeh, H., Nikoofard, A. Gas pipeline leakage detection based on sensor fusion under model-based fault detection framework. Journal of Petroleum Science and Engineering, 2020, 184: 106581.

Fedotov, Y. V., Belov, M. L., Kravtsov, D. A., et al. Selecting laser fluorosensor detection band to monitor oil pipeline leaks. IOP Conference Series: Materials Science and Engineering, 2021, 1155: 012074.

Fu, H., Yang, L., Liang, H., et al. Diagnosis of the single leakage in the fluid pipeline through experimental study and CFD simulation. Journal of Petroleum Science and Engineering, 2020, 193: 107437.

Ghosh, S., Saha, S. K. Modeling and simulation of subcooled coolant loss through circumferential pipe leakage. Journal of Nuclear Engineering and Radiation Science, 2021, 7(3): 034503.

Hudson, T. B., Follis, P. J., Pinakidis, J. J., et al. Porosity detection and localization during composite cure inside an autoclave using ultrasonic inspection. Composites Part A: Applied Science and Manufacturing, 2021, 147: 106337.

Jahanian, M., Ramezani, A., Moarefianpour, A., et al. Gas pipeline leakage detection in the presence of parameter uncertainty using robust extended Kalman filter. Transactions of the Institute of Measurement and Control, 2021, 43(9): 2044-2057.

Karthik, K., Jeyakumar, S., Sarathkumar, J. S. Optimization of wavy cylinder for aerodynamic drag and aeroacoustic sound reduction using computational fluid dynamics analysis. Proceedings of the Institution of Mechanical Engineers, Part C: Journal of Mechanical Engineering Science, 2021, 235(11): 1979-1991.

Keramat, A., Duan, H. F. Spectral based pipeline leak detection using a single spatial measurement. Mechanical Systems and Signal Processing, 2021, 161: 107940.

Lalitha, K., Balakumar, V., Yogesh, S., et al. IOT enabled pipeline leakage detection and real time alert system in oil and gas industry. International Journal of Recent Technology and Engineering, 2020, 8(5): 2582-2586.

Lu, H., Iseley, T., Behbahani, S., et al. Leakage detection techniques for oil and gas pipelines: State-of-the-art. Tunnelling and Underground Space Technology, 2020, 98: 103249.

Mahmutoglu, Y., Turk, K. Received signal strength difference based leakage localization for the underwater natural gas pipelines. Applied Acoustics, 2019, 153: 14-19.

Mei, Z., Yang, X., Liu, Z., et al. Study of pipeline leak detection and location method based on acoustic emission technology. Pipeline Technique and Equipment, 2021, 5: 17-21. (in Chinese)

Moosavi, S. R., Vaferi, B., Wood, D. A. Auto-detection interpretation model for horizontal oil wells using pressure transient responses. Advances in Geo-Energy Research, 2020, 4(3): 305-316.

Ning, F., Cheng, Z., Di, M., et al. A framework combining acoustic features extraction method and random forest algorithm for gas pipeline leak detection and classification. Applied Acoustics, 2021, 182: 108255.

Piltan, F., Kim, J. M. Advanced fuzzy-based leak detection and size estimation for pipelines. Journal of Intelligent & Fuzzy Systems: Applications in Engineering and Technology, 2020, 38(1): 947-961.

Quy, T. B., Kim, J. M. Leak detection in a gas pipeline using spectral portrait of acoustic emission signals. Measurement, 2020, 152: 107403.

Rai, A., Kim, J. M. A novel pipeline leak detection approach independent of prior failure information. Measurement, 2021, 167: 108284.

Sarallah, A., Mohammad, S. On the passive control of aeroacoustics noise behind a square cylinder. Journal of the

Brazilian Society of Mechanical Sciences and Engineering, 2021, 43: 58.

Shahmirzaee, M., Hemmati-Sarapardeh, A., Husein, M. M., et al. A review on zeolitic imidazolate frameworks use for crude oil spills cleanup. Advances in Geo-Energy Research, 2019, 3(3): 320-342.

Shan, L., Liu, Y., Tang, M., et al. CNN-BiLSTM hybrid neural networks with attention mechanism for well log prediction. Journal of Petroleum Science and Engineering, 2021, 205: 108838.

Shi, M., Ye, T., Zhou, B., et al. Design and experimental research of internal leakage detection device of buried pipeline ball valve based on valve cavity pressure detection. Flow Measurement and Instrumentation, 2022, 83: 102112.

Xu, C., Liu, P., Li, Z., et al. Leakage identification method of gas-liquid two-phase flow pipeline based on acoustic emission signal. Oil & Gas Storage and Transportation, 2021, 40(10): 1131-1137. (in Chinese)

Yuan, F., Zeng, Y., Luo, R., et al. Numerical and experimental study on the generation and propagation of negative wave in high-pressure gas pipeline leakage. Journal of Loss Prevention in the Process Industries, 2020, 65: 104129.

Zadkarami, M., Shahbazian, M., Salahshoor, K. Pipeline leak diagnosis based on wavelet and statistical features using Dempster-Shafer classifier fusion technique. Process Safety and Environmental Protection, 2017, 105: 156-163.

Zeng, Y., Luo, R. Numerical analysis on pipeline leakage characteristics for incompressible flow. Journal of Applied Fluid Mechanics, 2019, 12(2): 485-494.

Zhang, H., Yuan, G., Li, G., et al. Numerical simulation of leakage flow field for tubing and casing in gas wells. China Petroleum Machinery, 2020, 48(12): 123-129. (in Chinese)

Zhang, J., Lian, Z., Zhou, Z., et al. Acoustic method of high-pressure natural gas pipelines leakage detection: Numerical and applications. International Journal of Pressure Vessels and Piping, 2021a, 194: 104540.

Zhang, K., Tan, B., Zhang, W., et al. Design of a new acoustic logging while drilling tool. Sensors, 2021b, 21(13): 4385.

Zhang, M., Chen, X., Li, W. A hybrid hidden Markov model for pipeline leakage detection. Applied Sciences, 2021c, 11(7): 3138.

Zhang, T., Kou, J., Sun, S. Review on dynamic Van der Waals theory in two-phase flow. Advances in Geo-Energy Research, 2017, 1(2): 124-134.